Agricultural and Forest Meteorology 232 (2017) 265–278

Contents lists available at ScienceDirect

Agricultural and Forest Meteorology

journal homepage: www.elsevier.com/locate/agrformet

Identifying CO_2 advection on a hill slope using information flow

Minseok Kang[a], Benjamin L. Ruddell[b,*], Chunho Cho[c], Junghwa Chun[d], Joon Kim[a,e,f]

[a] National Center for Agro-Meteorology, 1, Gwanak-ro, Gwanak-gu, Seoul 08826, South Korea
[b] School of Informatics, Computing, and Cyber Systems, Northern Arizona University, S San Francisco St, Flagstaff, AZ 86011, USA
[c] National Institute of Meteorological Research, 33, Seohobuk-ro, Seogwipo-si, Jeju 63568, South Korea
[d] Department of Forest Conservation, National Institute of Forest Science, 57, Hoegi-ro, Dongdaemun-gu, Seoul 02455, South Korea
[e] Interdisciplinary Program in Agricultural & Forest Meteorology/Department of Landscape Architecture & Rural Systems Engineering, Seoul National University, 1, Gwanak-ro, Gwanak-gu, Seoul 08826, South Korea
[f] Institute of Green Bio Science and Technology, Seoul National University Pyeongchang Campus, 1447, Pyeongchang-daero, Deahwa-myeon, Pyeongchang 25354, South Korea

ARTICLE INFO

Article history:
Received 19 October 2015
Received in revised form 5 August 2016
Accepted 7 August 2016

Keywords:
Nighttime CO_2 flux correction
CO_2 advection
Forest hill slope
Eddy covariance measurement
Information flow
Dynamical process network

ABSTRACT

In hilly terrain affected by drainage flow, the horizontal advection of CO_2 makes it difficult to accurately observe the net ecosystem exchange of CO_2 by the eddy covariance technique. Downslope drainage can result in an overestimation of respiration at the bottom of a hill slope and an underestimation at the top, resulting in discrepancies among different flux corrections using filters based on the friction velocity, light response curve, and timing of advection. Vertical profiles of the CO_2 concentration from the ground to above the canopy were measured along with above-canopy EC flux measurements at the top and bottom of a hill slope at the Gwangneung KoFlux sites from 2008 to 2010. To infer the timing, direction, temporal scale, and structure of CO_2 advection from uphill to downhill, we constructed an information flow dynamical process network (DPN) based on the observed multi-level CO_2 concentrations. A site-specific quality control filter was developed to eliminate data strongly affected by CO_2 advection, which identifies the observations when strong downslope information flow exists in the DPN. This site-specific filter considerably reduced the discrepancies among different traditional flux corrections. This research provides a method for the general characterization of advection using information flow, and application of the method as a site-specific filter for eddy covariance observations in hilly and complex terrain.

1. Introduction

The main advantage of the eddy covariance (EC) technique is its direct measure of mass and energy exchange between the land surface and atmosphere. The quality of data measured by EC systems is assured (i.e., the measured flux represents the surface exchange) only if the measurement satisfies the conditions of dominant vertical turbulent transport and negligible horizontal and vertical advections (e.g., Baldocchi et al., 1988; Finnigan, 2004). At most flux sites, the quality of nighttime observations (particularly for CO_2 flux) is not acceptable because such conditions are not fulfilled. To address this issue, two types of approach are available (e.g., Aubinet, 2008). One is a 'correction approach' that adds the estimated correction terms (i.e., the sum of incoming and outgoing vertical/horizontal advective CO_2 fluxes). The other is a 'filtering approach' that identifies and discards the low quality data.

Most of the correction approaches are based on the direct measurement of advective CO_2 fluxes, for which multiple costly towers each featuring multi-level wind and CO_2 concentration profile systems are necessary (e.g., Leuning et al., 2008; Yi et al., 2008; Aubinet et al., 2010). However, the measurement system for advective CO_2 fluxes may not guarantee an acceptable estimation because some practical difficulties still remain (e.g., determining the control volume size and sampling resolution and ignoring horizontal turbulent transport). The magnitudes and patterns of advective CO_2 fluxes are site-specific, and it is therefore difficult to develop a general model for their estimation (e.g., Aubinet, 2008; Yi et al., 2008). For these reasons, filtering approaches are usually applied. There are various methods for filtering out poor quality CO_2 flux data such as the friction velocity (u^*) filtering method, advection-based filtering method, and light response curve method.

The most popular method is the u^* filtering method (hereafter, FVF) that estimates the parameters of the ecosystem respiration

* Corresponding author.
E-mail address: bruddell@asu.edu (B.L. Ruddell).

http://dx.doi.org/10.1016/j.agrformet.2016.08.003
0168-1923/

(RE) function (e.g., Lloyd-Taylor equation; Lloyd and Taylor, 1994) using the observed nighttime CO_2 flux when u^* is higher than a threshold, above which the dependency of the nighttime CO_2 flux on u^* fades away (e.g., Falge et al., 2001; Gu et al., 2005). When the nighttime CO_2 fluxes are underestimated or missing, the bad data are replaced with the data modeled using the air or soil temperature and the RE function with the estimated parameters. The FVF method cannot be used at sites where the u^* threshold cannot be identified and/or the drainage flow is developed at night, resulting in an underestimation of the CO_2 flux. van Gorsel et al., (2007, 2008, 2009) proposed a method (hereafter, VGF method) for hilly terrain sites affected by drainage flow using the observed CO_2 flux data from near sunset, when nighttime advection effect has not yet manifested (i.e., the maximum CO_2 flux data near sunset). However, for sites located in steep and complex topography where complex drainage wind systems develop, the VGF method is inadequate (van Gorsel et al., 2009). Alternatively, the light response curve method (hereafter, LRC) uses daytime CO_2 flux data and the y-intercept of the light response curve (as estimated daytime RE), which can be obtained from the regression of downward shortwave radiation (or photosynthetically active radiation) and daytime CO_2 flux (e.g., Lee et al., 1999). The LRC tends to underestimate RE because leaf respiration in light is reduced relative to that in darkness at the same temperature, particularly in deciduous forests (e.g., Brooks and Farquhar, 1985; Wohlfahrt et al., 2005; van Gorsel et al., 2009).

Typically, researchers use the appropriate method given their own site's necessary assumptions at any given time of day or year. These filtering approaches can lead to disagreement between multiple filtering approaches at any specific site or time when a filter's assumptions are violated. The difficulty involved in identifying the appropriate filter for a specific place and time motivates the development of filtering approaches that will work correctly at any specific site.

Gwangneung deciduous and coniferous sites in Korea (i.e., the GDK and GCK sites, respectively) are typical sites situated in hilly and complex terrain where the aforementioned filtering methods not only are difficult to apply correctly but also result in significantly different CO_2 fluxes (Kang et al., 2014). For example, the FVF cannot be applied properly due to the drainage wind system. The underestimation of RE from the LRC was not acceptable for the GDK because its magnitude was similar to the soil respiration independently measured by the chamber method (Lee et al., 2010; Chae, 2011; Lee, 2011). In this circumstance, the VGF method would be the most appropriate method for these sites, but the VGF results were also not acceptable because of the following discrepancies: (1) the magnitude of RE estimated by the VGF method for the GDK site located at the top of the hill slope (uphill) was smaller than that estimated by the FVF, which could have been underestimated by the drainage flow; (2) the magnitude of RE for the GCK site located at the bottom of a hill slope (downhill) was approximately twice that uphill; and (3) the magnitude of gross primary production (GPP) downhill was equivalent to the upper limit determined by solar radiation. Such results suggest that there is high probability that the nighttime drainage of CO_2 causes overestimation of respiration at the downhill site and underestimation of that at the uphill site (i.e., the CO_2 drained from the uphill site banks downhill at night). Furthermore, we can also speculate that the selected CO_2 flux data from the VGF method had already been affected by the drainage of CO_2 (i.e., the time at which CO_2 drainage developed was faster than that assumed by the method). The un-rotated vertical wind for the uphill changed to downdraft during the afternoon a couple of hours faster than that for the downhill, supporting our speculations (not shown). Therefore, to refine the filtering approach, a more site-specific approach is needed.

For sites with thermally induced mountain-valley circulation, the CO_2 concentration profile taken along the valley's flow streamline can provide information to help pinpoint the timing of CO_2 advection (e.g., Malla Thakuri et al., 2016). Such a mountain-valley circulation is dominant at the GDK and GCK sites (Hong et al., 2005; Yuan et al., 2007). These sites are located on the main streamline of the circulation, and the multi-level CO_2 concentration profiles are monitored to accurately estimate the storage flux (Hong et al., 2008; Yoo et al., 2009). The CO_2 concentration at each level of both sites varies with the magnitudes of sinks/sources (i.e., photosynthesis and respiration) and CO_2 transport (vertical and horizontal CO_2 fluxes). The data from the profile systems can be utilized to understand the characteristics of CO_2 drainage (e.g., Hong et al., 2008; Malla Thakuri et al., 2016). Profiles have advantages over EC fluxes in addressing this problem because the major source of nighttime net ecosystem exchange (NEE) is the soil surface, with the CO_2 accumulating to the soil surface, and the EC approach does not resolve fluxes under the canopy during calm nights.

The information flow dynamical process network (DPN) approach proposed by Ruddell and Kumar (2009a,b) can be used to statistically and robustly observe the presence of a horizontal advective coupling of CO_2 concentrations between two EC sites. The DPN was developed to analyze complex systems by delineating the couplings between observed system variables. Couplings are inferred by observing the time-lagged covariation using the theoretical information statistics such as the transfer entropy and quantifying the direction and strength of the coupling as an information flow. Based on the direction and strength of the information flow, we can attribute this to coupled process dynamics in this case of CO_2 advection, assuming that the differences in CO_2 dynamics between uphill and downhill are generated by the advective mass flows between the sites. The method is robust for this application because confounding non-advective processes affecting CO_2 dynamics between the two sites- such as microclimate differences- would need to be temporally correlated in a very precise and unlikely fashion in order to create a false-positive information flow between the sites.

The purpose of this study is to quantify an accurate carbon budget for sites located in hilly and complex terrain by ascertaining the effects of CO_2 drainage to CO_2 flux measured by an EC system (i.e., the sum of the observed vertical turbulent flux and storage term, F_{CO2_Obs}). We will accomplish this by applying a site-specific filter using the DPN method. Our specific objectives are (1) to develop the methods and necessary assumptions for the use of DPNs to characterize advection, (2) to qualitatively understand how the drainage-induced CO_2 advection affects the F_{CO2_Obs} and CO_2 concentration profile in a site with hilly and complex terrain based on the information flows, and (3) to provide a site-specific quality control filter with superior performance based on a hybrid of existing corrections applied with the appropriate filter for a given moment suggested by the DPN's characterization of advective drainage processes at that moment.

2. Materials and methods

2.1. Study sites

In Gwangneung National Arboretum, there are two flux towers in operation: the Gwangneung deciduous forest located at the top of a hill (GDK; 37° 45′ 25.37″ N, 127° 09′ 11.62″ E) and the Gwangneung coniferous forest located at the bottom (GCK; 37° 44′ 54.3″ N, 127° 09′ 45.3″ E) (Fig. 1(a)). Gwangneung is a royal forest that surrounds the mausoleum of King Sejo of the Chosun dynasty. Hence, over the last 500 years, this area has been protected to minimize human disturbance. Both sites are in a complex, hilly catchment (~220 ha) with a mean slope of 10–20°. The two towers are approximately 1.2 km apart, and the mean slope between

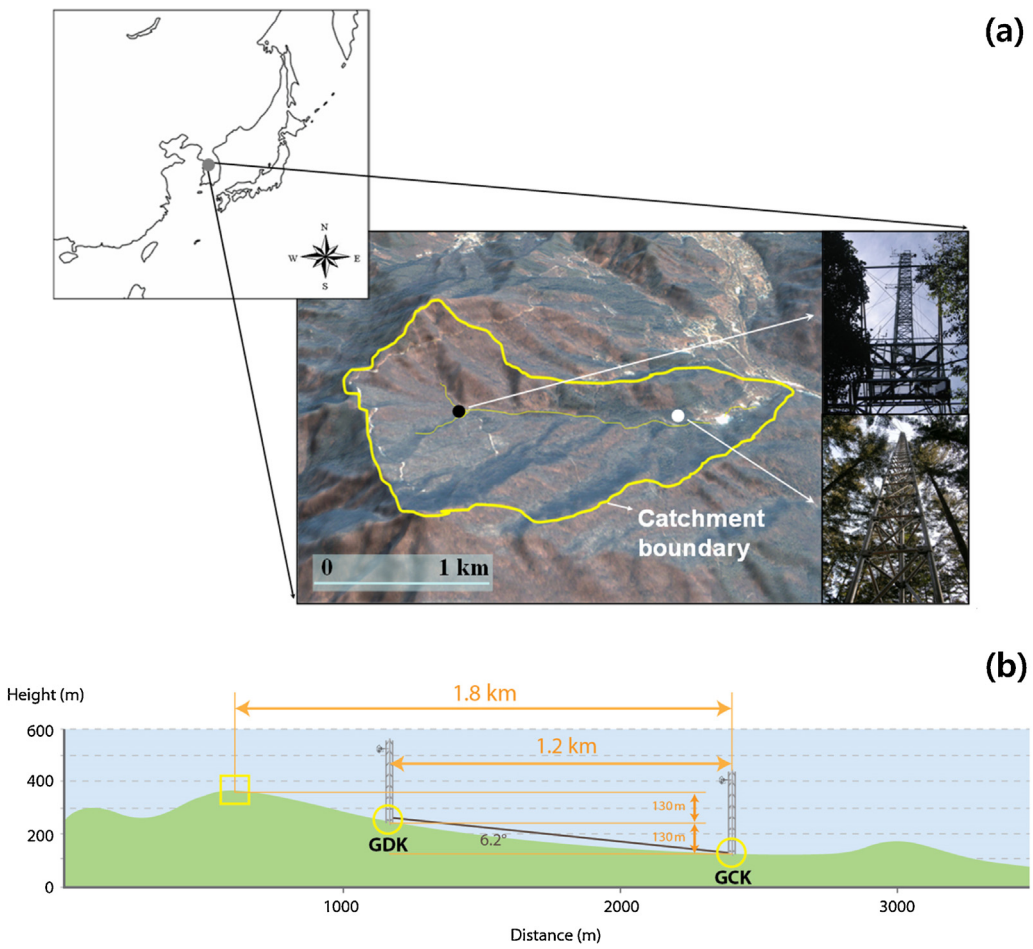

Fig. 1. Location of the Gwangneung KoFlux Supersite: the black dot indicates the deciduous forest (GDK) site, and the white dot indicates the coniferous forest (GCK) site (a). Cross-section of the Gwangneung forest watershed between the two flux towers (b, adapted from Moon et al., 2005).

the towers is approximately 6.2° (Fig. 1(b), Kim et al., 2006). The east/west slopes are gentle, whereas the north/south slopes are steep in the catchment. The thermally induced mountain-valley circulation is dominant in the GDK (uphill) and GCK (downhill) sites (Hong et al., 2005; Yuan et al., 2007). The 30-year climate normal was 11.5 °C for temperature and 1332 mm for precipitation (Hong et al., 2008). At the uphill site, the vegetation is dominated by an old natural forest of *Quercus* sp. and *Carpinus* sp. (80–200 years old) with a mean canopy height of ~18 m and a maximum leaf area index of ~6 in June. The downhill site is located in a generally lower and flat area compared to the uphill site and is a plantation forest with dominant species of *Abies holophylla* (less than 80 years old) with a mean canopy height of ~23 m and a maximum leaf area index of ~8 in June. The soil depth is 0.4–0.8 m, and the soil texture is mainly silty loam at the uphill site and sandy loam at the downhill site. Further descriptions of the sites can be found in Kim et al. (2006) and Kang (2013).

2.2. Measurements and data processing

The EC technique was used to measure the CO_2 flux from a 40-m tower at both sites. Vertical and horizontal wind speeds and temperature were measured with a three-dimensional sonic anemometer (Model CSAT3, Campbell Scientific Inc., Logan, Utah, USA) at 10 Hz at both sites. An open-path infrared gas analyzer (IRGA; Model LI-7500, LI-COR Inc., Lincoln, Nebraska, USA) was used at each site to measure water vapor and CO_2 concentrations. Half-hourly ECs and the associated statistics were calculated online from 10-Hz raw data and stored in dataloggers (Model CR-5000, Campbell Scientific Inc.). The corrections for ECs were done in the post-processing phase (see the Chapter 2.3 for more details). Other measurements such as net radiation, air temperature, humidity, soil temperature, ground heat fluxes, and soil water content were sampled every second, averaged over 30 min, and logged in the dataloggers (Model CR-3000 for the uphill site and CR-1000 for the downhill site, Campbell Scientific Inc.). More information about the EC and meteorological measurements can be found in Kwon et al. (2009), and Kang et al. (2009).

The multi-level profile systems were installed at both sites to measure the vertical profiles of CO_2 and H_2O concentrations and to estimate the storage flux in the control volume using a closed-path IRGA (Model: LI-6262, LI-COR Inc.; Hong et al., 2008; Yoo et al., 2009). The profile system, controlled by the dataloggers (Model CR-23X-TD, Campbell Sci. Inc.), was automatically calibrated on a daily basis for H_2O zero and CO_2 zero/span calibrations and manually calibrated on a weekly basis for H_2O and CO_2 zero/span calibrations. The measurement heights were 0.1, 1, 4, 8 (base of the crown), 12 (middle of the crown), 18 (the canopy top), 30, and 40 m for the uphill site and 0.1, 1, 4, 12 (base of the crown), 20 (middle of the crown), 23 (the canopy top), 30, and 40 m for the downhill site. The profile system visits each level once every 80 s. Measurements are made at each level for 10 s, but the last 4 s at each level are used to compute a level mean for purging the air from a previous level. The profile system uses miniature valves and minimizes the mixing of this common line with the adjoining passages. This leads to short equilibration time and fast cycle time to measure the concentra-

tions at all levels (Campbell Scientific Inc., 2003). For example, with orifice size 0.016 inch diameter, air intake flow rate of 1.3 SLPM and 49.26 kPa pressure in the sample cell of the IRGA, the settling time for 99.95% of the step change is 6 s for CO_2 when switching between two air steams with different CO_2 concentrations. The sampling rate was 4 Hz, and the averaging time was 30 min. More information about the multi-level profile system can be found in Hong et al. (2008) and Yoo et al. (2009).

2.3. Application of standard quality control, filtering, and correction methods

To improve the data quality by eliminating undesirable data, the collected data were examined by the quality control procedure based on the KoFlux data processing protocol (Hong et al., 2009; Kang et al., 2014, 2016). This procedure includes a sector-wise planar fit rotation (PFR; Make 8 tilt planes every 28-day; Wilczak et al., 2001; Yuan et al., 2007, 2011), WPL (Webb-Pearman-Leuning) correction (Webb et al., 1980), storage term calculation (Aubinet et al., 2001; Papale et al., 2006), spike detection (Papale et al., 2006), gap-filling (marginal distribution sampling method; Reichstein et al., 2005), and nighttime CO_2 flux correction (van Gorsel et al., 2009). The KoFlux protocol supports three different nighttime correction (i.e., filtering and replacing) methods: FVF, LRC, and modified VGF (van Gorsel et al., 2009; Kang et al., 2014, 2016).

These three filtering methods each have their own way of selecting good quality CO_2 flux data. The site-specific settings of the individual methods were as follows: (1) the u^* threshold for the FVF was 0.3 m s^{-1} for both the uphill and downhill sites based on the dependency of the nighttime F_{CO2_Obs} on friction velocity (constant regardless of season, Kang et al., 2014, 2016), (2) the Michaelis-Menten-type light response curve ($NEE = R_{LRCd} - (\alpha Q_t A_{max}/\alpha Q_t + A_{max})$, where R_{LRCd} is the estimated mean daytime RE, α is the apparent quantum yield, A_{max} is the canopy scale photosynthetic capacity, and Q_t is the total incident photosynthetically active radiation (PAR; in this study, we used downward shortwave radiation instead of PAR because PAR was not available) above the canopy; van Gorsel et al., 2009) was used for the LRC, and (3) the peak of F_{CO2_Obs} that occurred around sunset (R_{max}) was directly used for the modified VGF after calculating the median diurnal variation of the CO_2 flux for a certain period (Kang et al., 2014, 2016). The modified VGF produces a similar result to that from the original VGF for the sites. We applied a 30-day moving window to obtain the daily R_{LRCd} and R_{max}.

A_{max} varied over the season. A_{max} from LRC was less than 0.2 mg m^{-2} s^{-1} until early to mid-April and increased to ~2.2 mg m^{-2} s^{-1} around mid-July (i.e., before the monsoon) for the uphill site. During the monsoon, there was mid-season depression of A_{max} (~1.2 mg m^{-2} s^{-1}). A_{max} slightly recovered (~1.5 mg m^{-2} s^{-1}) after the monsoon (mid-August), and gradually decreased to ~1.0 mg m^{-2} s^{-1} in late-September. For the downhill site, A_{max} increased from ~0.3 mg m^{-2} s^{-1} (early-February) to ~1.9 mg m^{-2} s^{-1} (late-June). During the monsoon, A_{max} sharply decreased to ~1.5 mg m^{-2} s^{-1} and maintained until early October. A_{max} gradually decreased and reached its minimum of ~0.3 mg m^{-2} s^{-1} in mid-December.

The selected RE data from each filtering method were processed as follows. First, we estimate the parameters in the RE equation (Lloyd-Taylor equation, $RE = R_{ref}\exp\left(E_0\left(1/T_{ref} - T_0\right) - 1/(T_a - T_0)\right)$), where R_{ref} is the reference RE, T_{ref} is the reference temperature (=10 °C), E_0 is the activation energy parameter (°C^{-1}), T_0 is −46.02 °C, and T_a is the air temperature (°C), using the selected observed RE (Lloyd and Taylor, 1994). Second, we replace the bad (or missing) data with the calculated data using the air temperature and the RE function with the estimated parameters. Third, we estimate R_{ref} using an 30-day moving window which is shifted every 5-day in order to consider the variations of RE controlled by soil moisture and phenology, which is not accounted for in Lloyd-Taylor equation. This method cannot capture the temporal variation of RE controlled by soil moisture and phenology smaller than 5-days, but this is the dominant timescale of variation for soil moisture and is faster than necessary for phenology. The E_0 is constant for each site-year, which is estimated using the generic algorithm proposed by Reichstein et al. (2005) that derives a short-term temperature sensitivity (see Reichstein et al., 2005; Hong et al., 2009 for more details). GPP was calculated by subtracting NEE from RE.

2.4. Information flow dynamical process network (DPN) for CO_2 profiles

An information flow DPN is defined as a network of feedback loops and the associated time scales, where the variables in a system are cast as nodes and information flows as weighted directional links between nodes (Ruddell and Kumar, 2009a). The conjugation of the asymmetric information flows, in both magnitude and lag, between all pairs of variables in a system describes an information flow DPN (Kumar and Ruddell, 2010). The strength and time lag of directional information flow between two variables can be measured using transfer entropy (Schreiber, 2000).

Our hypothesis is that the drained CO_2 from the uphill banks up to the downhill at night. We expect to observe covariations of the mass rate in each layered control volume caused by the CO_2 advection between the sites. These covariations should be directional in space and time, corresponding to the direction and time scale of the advective flow. To describe the flows of CO_2 between the sites using the DPN approach, we define the DPN nodes as the rate of change of CO_2 mass in a layer of the control volume (m'^i and m'^j, ppm m per time step):

$$m'^i = \int \frac{\partial m^i}{\partial t} dz \approx \frac{\Delta m^i}{\Delta t}\Delta z^i,\ m'^j = \int \frac{\partial m^j}{\partial t} dz \approx \frac{\Delta m^j}{\Delta t}\Delta z^j \quad (1)$$

where m is the CO_2 mass in the layer, Δt is the time step (30 min in this study), Δz is the representative depth for each layer, and the superscripts i and j indicate the layers at the uphill and downhill sites, respectively. m'^i and m'^j are determined by the sum of fluxes, i.e., source/sink terms (s'^i and s'^j), vertical transport (w'^i and w'^j), and horizontal advection ($u_{net}{}'^i$ and $u_{net}{}'^j$) (Fig. 2):

$$\begin{aligned}
&m'^i = s'^i + w'^i + u_{net}{}'^i,\ m'^j = s'^j + w'^j + u_{net}{}'^j,\\
&s'^i = \int \frac{\partial s^i}{\partial t} dz \approx \frac{\Delta s^i}{\Delta t}\Delta z^i,\ s'^j = \int \frac{\partial s^j}{\partial t} dz \approx \frac{\Delta s^j}{\Delta t}\Delta z^j,\\
&w'^i = \int \frac{\partial w^i}{\partial t} dz \approx \frac{\Delta w^i}{\Delta t}\Delta z^i,\ w'^j = \int \frac{\partial w^j}{\partial t} dz \approx \frac{\Delta w^j}{\Delta t}\Delta z^j,\\
&u_{net}{}'^i = \int \frac{\partial u_{net}{}^i}{\partial t} dz \approx \frac{\Delta u_{net}{}^i}{\Delta t}\Delta z^i,\ u_{net}{}'^j = \int \frac{\partial u_{net}{}^j}{\partial t} dz \approx \frac{\Delta u_{net}{}^j}{\Delta t}\Delta z^j\\
&u_{net}{}^i = u_+{}^i + u_-{}^i,\ u_{net}{}^j = u_+{}^j + u_-{}^j
\end{aligned} \quad (2)$$

where s, w, and u are the CO_2 mass generated/transferred in/to the layer by photosynthesis/respiration, vertical transport, and horizontal transport, respectively, and the subscripts +, −, and *net* indicate the incoming, outgoing, and net flows, respectively. We quantify the information flows from uphill to downhill (and vice versa) yielding 128 pairwise combinations of information flows between the eight vertical layers at the two sites (i.e., $m'^i \rightarrow m'^j$ and $m'^j \rightarrow m'^i$).

To quantify the relative magnitude of CO_2 advection by season, we divide the dataset seasonally according to the phenology based on the plant area index (Kang et al., 2012; Kang, 2013): (1) dormant (December, January, February, and March), (2) transition (April, May, October, and November), and (3) growing (June, July, August,

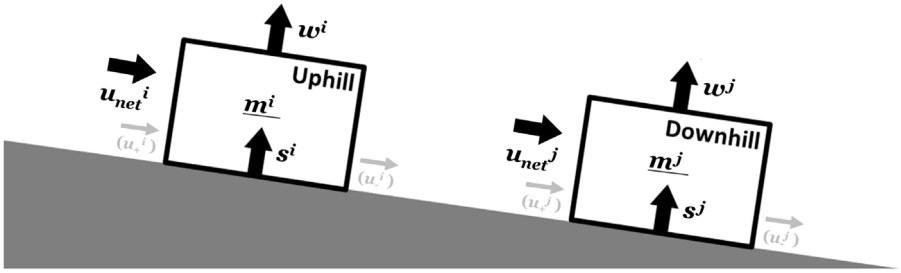

Fig. 2. Simplified two-dimensional diagram of the CO_2 mass balance in a layer of the control volume for the study sites under drainage flow. m is the CO_2 mass in the layer; s, w, and u are the CO_2 mass generated/transferred in the layer by photosynthesis/respiration, vertical transport, and advection, respectively; the superscripts i and j indicate the layers at the uphill and downhill sites, respectively; and the subscripts +, −, and *net* indicate the incoming, outgoing, and net flows, respectively.

and September) seasons. To identify the timing of CO_2 drainage, we calculate the information flows between all of the m's every hour using an eight-hour moving window. Eight hours is the smallest window we can use because of minimum sample size which guarantees a robust estimation of the theoretical information statistics (more details are explained later).

m' varies dynamically with the magnitudes of horizontal/vertical CO_2 transport and photosynthesis/respiration (See Eq. (2)). The dominant time scales in the process of photosynthesis/respiration (mainly controlled by solar radiation and air/soil temperature) are diurnal and annual. Significant sub-diurnal variability is detectable with EC down to approximately 30 min (e.g., Baldocchi et al., 2001). The dominant time scale in the process of CO_2 drainage is sub-diurnal at less than eight hours. To boost the sub-diurnal drainage dynamics and suppress slower dynamics (i.e., photosynthesis/respiration), we apply a high-pass Fourier transform filter at eight hours (similar to using the five-day synoptic anomaly transformation in Ruddell and Kumar (2009a)) to the observed signal. However, we speculated that significant photosynthesis/respiration signals would remain and their effects would be greater in the growing season.

The transfer entropy is based on the dynamical Shannon entropy (H, Shannon, 1948) or information entropy of a time series. $H(X_t)$ is the summation across the marginal probability function $p(x)$ of all discretely defined states x of time series variable X_t as:

$$H(X_t) = -\sum_{x} p(x)\log(p(x)). \tag{3}$$

Transfer entropy ($T(X_t{}^{(i)} \to X_t{}^{(j)},\tau)$) measures the reduction in the Shannon entropy of variable $X_t{}^{(j)}$ based on the knowledge of prior-state τ time steps earlier in another variable $X_t{}^{(i)}$, which is in addition to the information provided by the immediate prior history of $X_t{}^{(j)}$ (Schreiber, 2000; Ruddell and Kumar, 2009a; Kumar and Ruddell, 2010). This is estimated using the joint and conditional probabilities as follows:

$$T(X_t^{(i)} \to X_t^{(j)}, \tau) = \sum_{x_t^{(j)}, x_{t-\Delta t}^{(j)}, x_{t-\tau\Delta t}^{(i)}} p(x_t^{(j)}, x_{t-\Delta t}^{(j)}, x_{t-\tau\Delta t}^{(i)}) \log \frac{p(x_t^{(j)} | (x_{t-\Delta t}^{(j)}, x_{t-\tau\Delta t}^{(i)}))}{p(x_t^{(j)} | x_{t-\Delta t}^{(j)})}. \tag{4}$$

Transfer entropy ignores dynamics shared by a pair of variables and measures the unique statistical information provided by one variable to the other at a process time scale, τ. We use the normalized form $T' = T/\log(M)$, where $\log(M)$ is the upper bound in the estimate of entropy $H(X_t{}^{(i)})$ for $X_t{}^{(i)}$ using M discrete bins for the estimation of the probability distribution function.

For the typical flux tower data (i.e., air/soil temperature, vapor pressure deficit, solar radiation, precipitation, soil water content, sensible/latent heat flux, and carbon fluxes), Ruddell and Kumar (2009a) proposed that M = 11–20 bins and the number of pairs N > 500–1000 is a good rule of thumb for the application of transfer entropy using finite-interval bin-counting probability density estimation schemes to obtain a qualitatively consistent result. Under the condition of using an eight-hour moving window and dividing into the three seasons, the N of m' from 2008 to 2010 ranged from 3500 to 5000. However, despite this larger N, $T'(m'^i \to m'^j, \tau)$ and $T'(m'^j \to m'^i, \tau)$ were overestimated using M = 11–20 bins in this case. Theoretically, $T'(m'^i \to m'^j, \tau)$ should be bounded by its mutual information ($I'(m'^i \to m'^j, \tau)$; Ruddell and Kumar, 2009a). Accordingly, we use M = 6 bins to suppress overestimation because we are unable to increase N. It appears that quantitatively accurate $T'(m'^i \to m'^j, \tau)$ estimates require significantly larger N, whereas qualitative accuracy can be achieved according to the experiment for estimation of entropy statistics using various N and M in the previous study (see Appendix A in Ruddell and Kumar, 2009a). We define the minimum observable dynamics magnitude (Ω, i.e., bin width) as 50 ppm m per time step (which corresponds to ~0.05 mg m^{-2} s^{-1}, time step: 30 min) and the bin edges as [−150, −100, −50, 0, 50, 100, 150] in this case. All of the values beyond an absolute boundary of 150 ppm m per time step (extremely low probability, 0.43% of the total) were included in the first/last bins. The dynamics of m' smaller than the 50 ppm m per time step of Ω at time scale τ will not be captured. The choice of Ω represents a balance between physical detail and numerical quality, given the datasets' time step (Δt) and the process time scale τ.

$T'(m'^i \to m'^j, \tau)$ is computed for each of the four time lags between one half of an hour and two hours. Then, we can statistically describe the information flow due to the advective CO_2 flows between the sites in the time scale of greater than or equal to one half of an hour and less than or equal to two hours. One half of an hour is a minimum resolution for our EC and profile measurements (Δt), and two hours is the largest τ that can guarantee a robust numerical estimation of $T'(m'^i \to m'^j, \tau)$ with sufficient N.

To quantify the average information flow due to advective CO_2 drainage from uphill to downhill, we integrate the transfer entropy over the layers as $\sum_{i,j} T'(m'^i \to m'^j, \tau)$ (hereafter $\Sigma T_{down}{}'$). Similarly, we can define the integrated T' from downhill to uphill as $\Sigma T_{up}{}'$.

To establish statistical significance of the calculated T', i.e., whether a T' is significantly stronger than that which would occur through random chance between unrelated time series, Ruddell and Kumar (2009a) used the method of shuffled surrogates. To estimate the shuffled surrogate transfer entropy $T_{ss}{}'$, the values of time series X_t and Y_t are shuffled randomly in time to destroy the time correlations between them, forming new time series' X_{ss} and Y_{ss}. The surrogate transfer entropy $T_{ss}{}'$ ($X_{ss} \to Y_{ss}$) is computed for several realizations using Monte Carlo simulations, resulting in a Gaussian distribution of surrogates with mean ($\mu(T_{ss}{}')$) and standard deviation ($\sigma(T_{ss}{}')$). In this study, we use the upper boundary of the 95% confidence level (Δ) with 100 Monte Carlo simulations. We do not consider the two statistics for each link because we are evaluating the total strength from uphill to downhill (and vice versa), not the switching of each coupling. Therefore, to identify the timing

of CO_2 advection, we use the integrated Δ (i.e., $\Sigma\Delta_{down}$ and $\Sigma\Delta_{up}$) with links similar to the integrated T' (i.e., $\Sigma T_{down}'$ and $\Sigma T_{up}'$).

In summary, to robustly identify mass advection as a dynamical information flow, the following numerical and physical conditions should be satisfied:

(1) Dissimilar system states (i.e., different strengths and vectors of advection) are not mixed in a dataset or blended in a single DPN; this can be achieved based on prior knowledge or by statistical optimization.
(2) The number of data (N) is large enough to calculate an accurate DPN; this can be achieved by increasing the bin width (Ω), improving the numerical schemes, or using larger samples without mixing the system states.
(3) The bin width Ω must not be larger than the average magnitude of m' at the advection process's time scale τ at which the two locations are linked by advection (i.e., $\Omega \leq |\Delta m|\Delta z/\tau$, recall that $\tau \geq \Delta t$, so if $\tau = \Delta t$, $\Omega \leq |m'|$); this can be achieved by decreasing Ω.
(4) The mass rate of advection (u_{net}'), on average, is of greater or equal magnitude to the net mass rate of orthogonal transports (i.e., the sum of vertical transport (w') and photosynthesis/respiration of CO_2 (s')); in this case, $|u_{net}'| \geq |w' + s'|$, so that $T'(u_{net}'^{i} \rightarrow u_{net}'^{j}, \tau)$ can be estimated as $T'(m'^{i} \rightarrow m'^{j}, \tau)$; this can be achieved by filtering out the effect of w' and s' on m', or by choosing system states where w' and s' are small or $w'^{i} \approx w'^{j}$ and $s'^{i} \approx s'^{j}$, or $w'^{i} + s'^{i} \approx w'^{j} + s'^{j}$.

To satisfy condition (1), we divide the dataset seasonally and sub-daily based on prior knowledge of the state of the mountain-valley circulation. When the number of available data and its boundary are fixed, conditions (2) and (3) are concatenated with each other. As mentioned before, we use $M = 6$, corresponding to $[-150, -100, -50, 0, 50, 100, 150]$ of the bin edges, and the resolved advection dynamics are greater than 50 ppm m per time step, on average, at the process time scale τ. Considering that our purpose is to quantify the relative magnitude of CO_2 advection between the sites, the accuracy of the DPN is acceptable in this case.

Before regarding condition (4), we recall that the vertical transport term w' consists of the vertical turbulent transport and vertical advection. In the case of the vertical turbulent transport, it is negatively correlated with $|u_{net}'|$ that $|u_{net}'|$ enhances in calm conditions, while the vertical turbulent transport weakens (e.g., Hong et al., 2008). On the contrary, there is not a general relationship between $|u_{net}'|$ and vertical advection: direct advection measurements were performed at several sites, but the patterns of horizontal and vertical advections were shown to be strongly site dependent (e.g., Aubinet, 2008; Feigenwinter et al., 2004; Marcolla et al., 2005; Novick et al., 2014). The vertical advection might be greater than the horizontal advection in the growing season with high leaf area index due to sizable vertical CO_2 density gradient. Thus, it is hard to argue that the horizontal advection is dominant compared to the vertical advection for the study sites without direct advection measurements.

However, the methods presented here are not necessarily confounded by a large vertical advection. These methods are statistical, and assume that the vertical advection at each of the two sampling points (i.e., each of the pairwise combinations between the eight vertical layers at the two sites) has a peak cross-correlation time lag of zero (i.e., maximally correlated at zero lag). In other words, we require that the vertical advections are not mutually cross-correlated nor correlated with the horizontal advection at the same or at the other sampling point at a time lag significantly larger than zero. Such a time lagged cross-correlation could, if it were strong enough and if it occurred at time lags similar to the time lags corresponding to those of the horizontal advection, then confound a robust indication of horizontal advection. We have no reason to believe this to be the case at this site. Instead, it is our judgment based on canopy structure that the vertical advection terms at the two sampling points are nearly synchronized with cross-correlations peaking a near-zero lags.

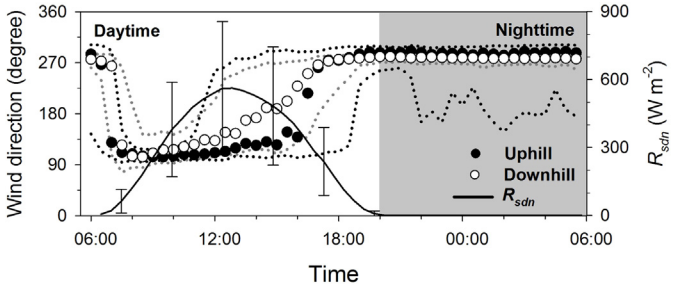

Fig. 3. Median diurnal variation of wind direction and mean diurnal variation of downward shortwave radiation (R_{sdn}) for the uphill (GDK) and downhill (GCK) sites during the growing season (i.e., June–September). The shaded area represents nighttime (i.e., when R_{sdn} is equal to 0 W m^{-2}), and the unshaded area represents daytime (i.e., when R_{sdn} is larger than 0 W m^{-2}). The error bars indicate the standard deviation for each half hour. Dotted lines indicate diurnal variations of the first and third quartiles of wind direction for the uphill (black) and the downhill (grey).

As mentioned above, we boost the signal from advection and suppress that from photosynthesis/respiration to satisfy this condition. Although $s' > u_{net}'$, if the dynamics of s'^{i} and s'^{j} are identical, we can extract the signal of the advection between the site by calculating net $\Sigma T'$ (i.e., $\Sigma T_{down}' - \Sigma T_{up}'$, hereafter $\Sigma T_{net}'$). Air temperature is a primary driver of respiration, so differences in air temperature between the sites can affect respiration rates. The air temperature is warmer during the day but cooler during the night at the downhill site, e.g., the range of mean diurnal variation at the downhill is about 2 °C. larger that at the uphill during the growing season. However, the information flow method we employ is sensitive to temporal cross-correlations in observations, not the observed values themselves. The dynamics (i.e., temporal patterns of change) of air temperature at the two sites are synchronized even though the temperatures at the two sites differ; in other words, the time cross-correlation of the two sites' temperatures peaks at a time lag of zero. In addition, downward shortwave radiations are almost identical, and there is a little bias in H_2O concentration between the sites. The methods are therefore robust and nonsensitive to differences in the temperature, radiation, and water forcings between the two sites. We test the methodology for a synthetic example and its result is provided in Appendix A to provide additional evidence for the robustness of the methods in identifying the strength and direction of advection between two locations.

3. Results and discussion

3.1. Effects of drainage flow on CO_2 concentration and flux

Fig. 3 shows the mean diurnal patterns of wind directions for the uphill (GDK) and downhill (GCK) sites for the growing season. The mountain winds blew at night (including sunrise and sunset), whereas the valley winds blew during the day. Similar diurnal patterns occurred in the other seasons, except that the duration of valley wind decreased with the length of day (not shown). These thermally induced mountain-valley circulations affected the dynamics of the concentrations and fluxes of CO_2, as observed in Figs. 4 and 5.

We note a few interesting features in the seasonally averaged diurnal patterns of CO_2 concentrations near the surface, near the canopy top, and at 40 m for both the uphill and downhill sites (Fig. 4; see Malla Thakuri et al. (2016) for more detailed information of

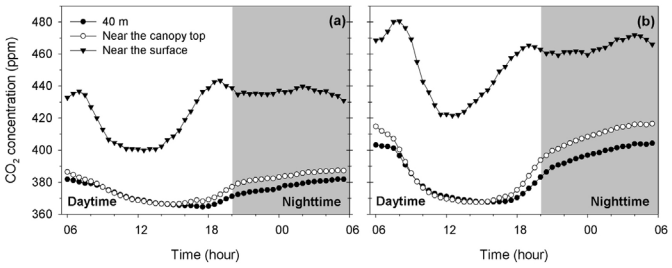

Fig. 4. Mean diurnal variation of CO_2 concentrations near the surface, near the canopy top, and at 40 m for the uphill (GDK; a) and downhill (GCK; b) sites during the growing season (i.e., June–September). The shaded areas represent nighttime, and the unshaded areas represent daytime.

the concentration profiles at the sites). First, near the canopy top and at 40 m, the diurnal ranges of the CO_2 concentrations downhill were more than two-fold greater than those uphill. Such a difference is too large to be attributed solely to the higher photosynthetic/respiratory capacity of the coniferous stands at the downhill site, which are taller, denser, and younger, and ~2 °C larger range of diurnal variation of air temperature. This yields ~0.02 mg m^{-2} s^{-1} per °C estimated from the temperature response function of RE using the Lloyd-Taylor equation. We speculate that there must have been an additional contribution, such as CO_2 drainage. Scrutiny of the above-mentioned diurnal patterns suggests that the drained CO_2 from the uphill banks up to the downhill areas, particularly during sunset when the differences in the time rate of change in CO_2 concentrations between the two sites were largest. Second, the nighttime CO_2 concentrations near the ground, which are supposed to increase continuously, did not increase but fluctuated. Fig. 4 indicates that CO_2 drainage was occurring at both the uphill and downhill sites. Particularly at the uphill site, we observe that the CO_2 concentrations decreased at night.

Fig. 5 shows the mean diurnal variations of the F_{CO2_Obs} and storage term for the uphill and downhill site during the growing season. The data are presented using all of the data (Fig. 5a) and the data under high u^* conditions (i.e., when the vertical turbulent transport is dominant compared to storage and advection terms; Fig. 5b). In Fig. 5a, the F_{CO2_Obs} was maximal around sunset and rapidly dropped at both sites. The F_{CO2_Obs} maxima at the downhill and uphill site showed differences of a factor of two, while such a difference was not observed under high u^* conditions (Fig. 5b). These results suggest that the peak F_{CO2_Obs}s in Fig. 5a underestimate (overestimate) the true NEE (in the absence of CO_2 drainage) for the uphill (downhill) sites. Additionally, the storage term showed obtrusive peaks around sunset and early morning for the downhill site (Fig. 5a), which was not observed under high u^* conditions (Fig. 5b), thereby explaining the above-mentioned under/overestimation of NEE. Moreover, the F_{CO2_Obs} around sunrise was much smaller than that around sunset, despite the similar magnitudes of downward shortwave radiation (R_{sdn}) for both periods (see Fig. 5). Air temperature is typically much colder at sunrise than sunset, which could explain smaller F_{CO2_Obs} in the morning, though it does not explain ~0 of F_{CO2_Obs} in the morning. Considering that the mountain wind continued until an hour and a half after sunrise, the CO_2 drainage must have persisted around sunrise. Even under high u^* conditions, the differences in F_{CO2_Obs} between sunset and sunrise periods were still present, though smaller. This finding is not an artifact of the choice of coordinate rotation because these findings also emerge after making a simple coordinate rotation (McMillen, 1988).

In summary, we have identified the different patterns of CO_2 concentrations between the uphill and downhill site and the underestimation (or overestimation) of the peak F_{CO2_Obs}s, supporting our hypothesis that the drained CO_2 from the uphill site banks up to the downhill site. However, the CO_2 drainage could begin a couple of hours before sunset and persist until an hour and a half after sunrise. The overestimation of NEE (hence, making a stronger carbon sink) at the downhill site during the morning hours may be attributed to the dissipation (probably vertical turbulent transport) of the banked CO_2 at the site. The significant negative CO_2 storage term at the downhill site further substantiates this observation during this period.

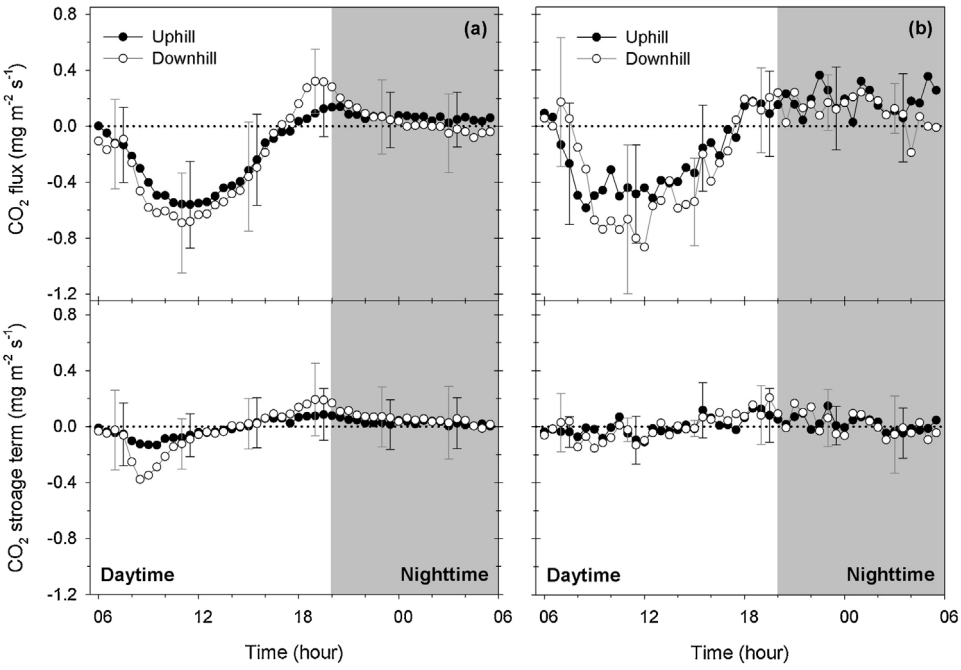

Fig. 5. Mean diurnal variations of the observed CO_2 fluxes and storage terms for the uphill (GDK) and downhill (GCK) sites during the growing season (i.e., June–September) using (a) all of the data and (b) the data under high u^* conditions (i.e., both daytime and nighttime averages of u^* were greater than the threshold value of 0.3 m s^{-1}). The error bars indicate the standard deviation for each half hour. The shaded areas represent nighttime, and the unshaded areas represent daytime.

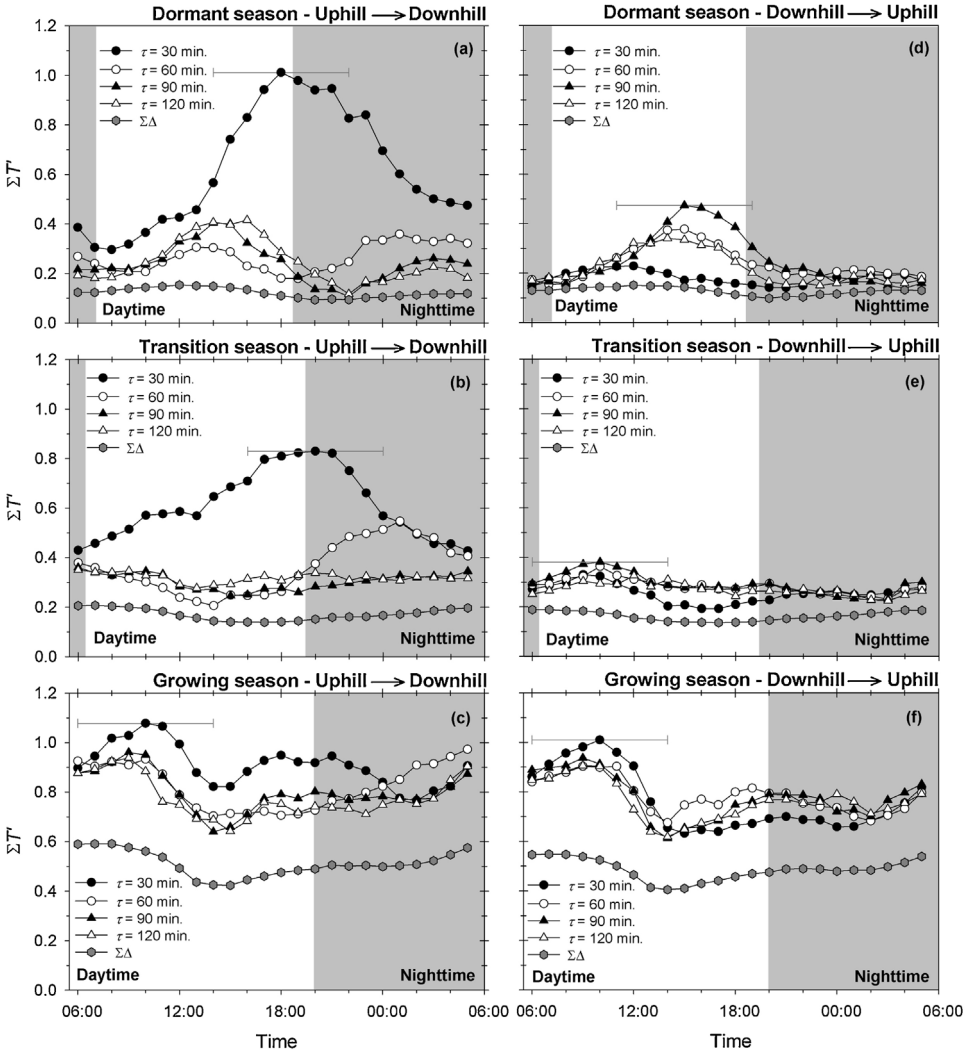

Fig. 6. Diurnal variation of the integrated transfer entropy ($\Sigma T'$) of CO_2 from uphill (GDK) to downhill (GCK) with time lags (uphill → downhill; a–c) and vice versa (downhill → uphill; d–f) and the statistical significance (Δ) by season (i.e., dormant season: December, January, February, and March; transition season: April, May, October, and November; growing season: June–September). The horizontal bars indicate the time window size for quantifying $\Sigma T'$ (8 h). The shaded areas represent nighttime, and the unshaded areas represent daytime.

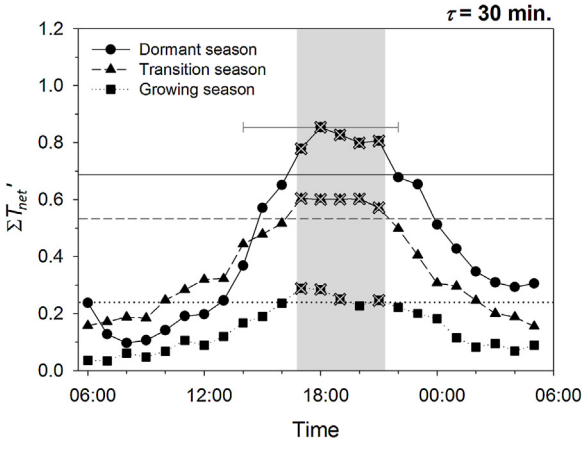

Fig. 7. Diurnal variation of the net integrated transfer entropy of CO_2 ($\Sigma T_{net}'$) from uphill (GDK) to downhill (GCK) with a half-hour time lag. The horizontal bar indicates the time window size for quantifying $\Sigma T_{net}'$ (8 h). X marks indicate a $\Sigma T_{net}'$ larger than the empirical criterion (C_E). Each horizontal line indicates the C_E for the season (solid line for the dormant season, dashed line for the transition season, and dotted line for the growing season). The shaded area represents the period when $\Sigma T_{net}'$ is larger than C_E.

3.2. How did the drained CO_2 from the uphill site accumulate downhill?

To identify the timing, direction, relative strength, temporal scale, and structure of CO_2 advection from uphill to downhill, we calculated the information flow DPN of CO_2 for all the layers. Fig. 6 shows the diurnal variation of the layer-integrated transfer entropy from uphill to downhill with time lags ($\Sigma T_{down}'$; Fig. 6a–c) and vice versa ($\Sigma T_{up}'$; Fig. 6d–f) by season (i.e., dormant, transition, and growing). There are several peaks in the $\Sigma T'$ that can be divided into the peaks appearing only in the direction from uphill to downhill (e.g., $\Sigma T_{down}'$s with a half hour time lag around sunset and $\Sigma T_{down}'$s with one hour time lag around midnight) and the peaks appearing bidirectionally (e.g., $\Sigma T'$s at approximately 14:00 in the dormant season and $\Sigma T'$s at approximately 9:00 in the transition and growing seasons). The former could be associated with CO_2 advection from uphill to downhill, whereas the latter could be associated with turbulent mixing and photosynthesis/respiration, which are controlled by micrometeorological conditions (e.g., wind, solar radiation, and air temperature). All of the $\Sigma T'$s are statistically significant, suggesting that a significant signal associated with turbulent mixing and photosynthesis/respiration would remain after

the high-pass filtering. Hereafter, we do not consider the peak of one-hour time lag at approximately midnight because we do not focus on the process during and after midnight when the drainage flow is fully generated.

Assuming that the T' values associated with turbulent mixing and photosynthesis/respiration are almost identical between the sites, we calculated the $\Sigma T_{net}{}'$ from uphill to downhill with a half-hour time lag to quantify the information flow induced by CO_2 advection between the sites (Fig. 7). The timing when the $\Sigma T_{net}{}'$ is higher than its C_E (empirical criterion) is from 17:00 to 21:00 regardless of the season, indicating a peak in downslope-advected CO_2 at that time. This is almost identical to the timing of the emergence of the differences in the F_{CO2_Obs} and storage term of CO_2 between the sites (see Fig. 5). However, contrary to our expectations, the transitional period from the dormant season to the growing season results in a smaller $\Sigma T_{net}{}'$, which may be because the magnitude of dynamics associated with horizontal CO_2 advection is smaller than that due to photosynthesis/respiration and vertical advection during the growing season (i.e., the physical conditions of our method are not completely satisfied; see the Chapter 2.4 for more details).We cannot observe a negative value in $\Sigma T_{net}{}'$ during the morning, indicating that the accumulated CO_2 in the downhill site did not dissipate to the uphill site.

Additionally, we could estimate the mean information flow velocity of the CO_2 drainage as ~0.67 m s^{-1} through a simple calculation (i.e., 1200 m of the distance between the sites divided by 1800s of the half-hour time lag) to be slightly higher than the mean vertically averaged west-east direction wind velocity from 17:00 to 21:00 at the uphill site during the study period ; ~0.54 m s^{-1}, estimated using 1.03 m s^{-1} of the mean observed velocity at 40 m and the theoretical wind profile equations, i.e., $u(z) = u^*/0.4 \ln[(z-d)/z_m]$ for above the canopy and $u(z) = u(h)\exp[a(z/h-1)]$ for within the canopy, where $u(z)$ is the wind speed (m s^{-1}) at the height z (m), u^* is the frictional velocity (m s^{-1}), h is the canopy height (m), d is the zero plane displacement (= 0.75 h, in this study), z_m is the roughness length (= 0.1 h, in this study), and a is the attenuation coefficient (= 1, in this study); Campbell and Norman (1998). This calculation could be affected by the discrete time step of 30 min and also by the shape of the wind profile, both of which likely differ under advective conditions as an under-canopy secondary maximum advection layer develops. However, we find no evidence of this confounding effect, because the time lag of peak information flow (i.e., time scale of CO_2 advection from uphill to downhill) does not change with the height (at least not more than the half-hour time resolution of the analysis).

We also identify the vertical structure of CO_2 advection from uphill to downhill using the non-integrated net transfer entropy. Fig. 8 shows the vertical structure of the normalized (i.e., the minimum subtracted, divided by the difference between the minimum and the maximum for each season) net transfer entropy of CO_2 with a half-hour time lag near the sunset peak of 18:00 by season. In the dormant season when there are no leaves in the deciduous forest (uphill), the CO_2 flows are predominant from all vertical layers of the uphill site to below the canopy downhill. The closer the period is to the growing season (i.e., the more the canopy is developed), the more clearly the CO_2 flows are divided into two parts, i.e., above and below the canopy.

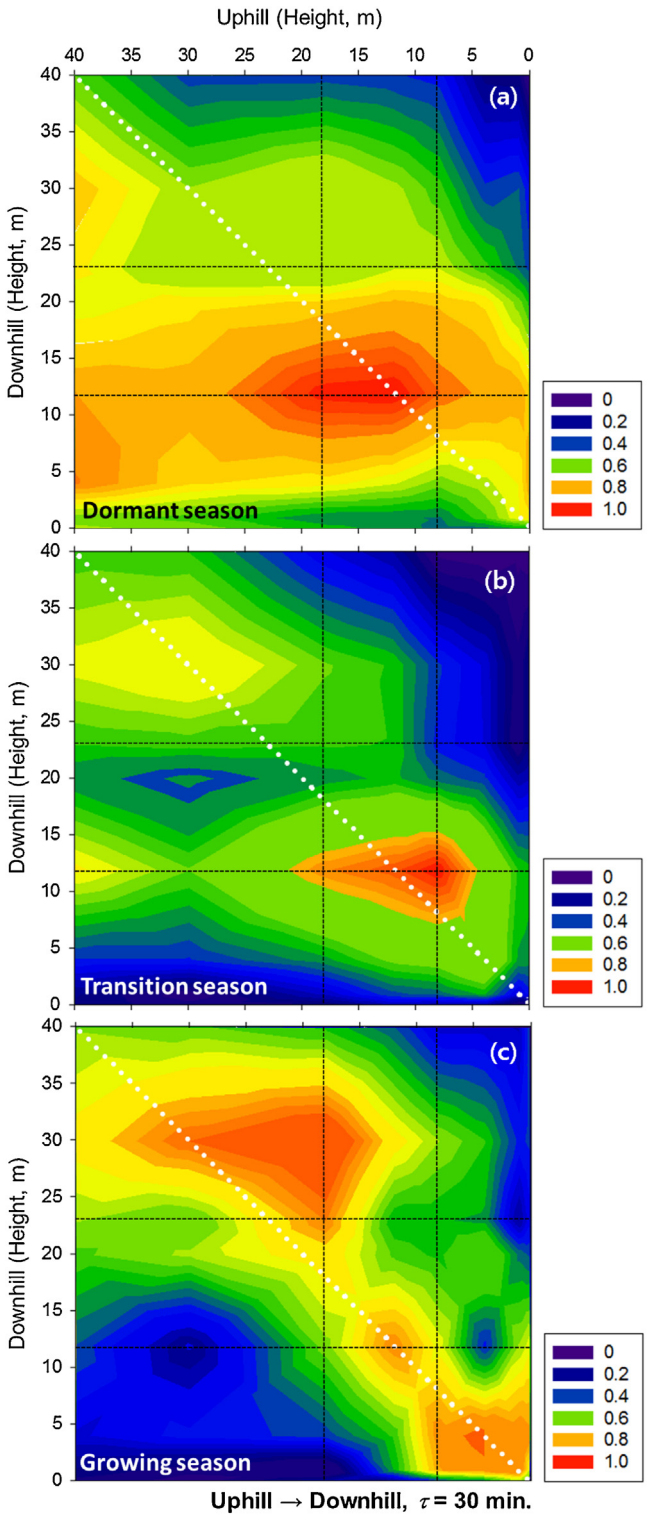

Fig. 8. Vertical structure of non-integrated normalized net transfer entropy of CO_2 between the study sites with a half-hour time lag at approximately 18:00 by season (i.e., dormant season: December, January, February, and March; transition season: April, May, October, and November; growing season: June–September). The white and black dotted lines represent the 1:1 line and the heights of the canopy top and bottom, respectively.

3.3. *Filtering advection-affected eddy covariance (EC) data using the advection DPN*

The CO_2 drainage from uphill to downhill peaks between 17:00 and 21:00 based on the information flow DPN of CO_2 between the sites (in other words, CO_2 is accumulating downhill from an uphill source). Thus, we should filter out the F_{CO2_Obs} that is

under/overestimated due to the CO_2 drainage from approximately 17:00 to 21:00 before applying the nighttime CO_2 flux correction.

The traditional u^* threshold (0.3 m s^{-1} for the sites; Kang et al., 2014, 2016) has the ability to filter out the poor quality data from 17:00 to 21:00 in the previous section (see Fig. 5). Yi et al. (2008) also reported that the magnitude of advective flux associated with downslope katabatic flow decreased with increasing u^*, using a measurement approach consisting of multiple towers. To verify that u^* can still be used for the filtering approach around sunset, we simply quantify the $\Sigma T_{net}'$ at approximately 18:00 for the two subsets, which are divided into using the averaged u^* for the uphill and downhill sites and 0.3 m s^{-1} of the u^* threshold, despite the overestimation of transfer entropy due to an insufficient number of data. The $\Sigma T_{net}'$s under the higher u^* condition (i.e., higher than 0.3 m s^{-1}) are 65%, 26%, and 37% lower than those under the lower u^* condition (i.e., lower than 0.3 m s^{-1}) for the dormant, transition, and growing seasons, respectively, which supports the application of the u^* threshold to filter out the poor quality data around sunset. According to all of the findings, we propose an additional site-specific quality control filter for discarding drainage-affected EC observations as follows.

1) Discard the data from the time at which the drainage flow has been fully generated (when the most of drained CO_2 from the uphill site does not bank up to the downhill site but passes through the downhill site and flows into the end of hill slope, 21:00 in this study) to the time at which the mountain wind changes to the valley wind after sunrise (9:00, 8:00, and 7:30 for the dormant, transition, and growing seasons, respectively).
2) Discard the data when u^* is lower than the threshold (0.3 m s^{-1}) while the drainage flow is under strong development (from 17:00 to 21:00). For the downhill data, consider the u^* for not only the downhill but also the uphill in advance of the significant CO_2 information flow time lag (30 min) as a data filter.
3) Discard the data during all mornings for the downhill site because the data includes the dissipation of the drained CO_2 from the uphill site and may overestimate the true NEE.

This site-specific filter is based on a theoretical background similar to the nighttime corrections, i.e., FVF and VGF methods. Thus, the site-specific filter has the equivalent effect of needing to apply two (or three) nighttime correction methods in a hybrid way. These procedures can be applied to other sites if we can estimate the timing and duration of the CO_2 drainage from uphill to downhill and the u^* threshold at that time.

Table 1 shows the improved annual CO_2 budget from the time of application of the site-specific filter. For the FVF method, the RE generally increases for both sites after the application of the site-specific filter because the underestimated nighttime F_{CO2_Obs}s due to the drainage flow are not included in the estimation of the parameters of the Lloyd-Taylor equation. It also suggests that the incoming drained CO_2 from uphill to downhill was lower than the outgoing drained CO_2 from the downhill site at night ($u_+{}^j - u_-{}^j = u_{net}{}^j < 0$, see Eq. (2)).

For the LRC method, the RE and GPP increase enormously at both sites after the application of the site-specific filter. In particular, the RE for the uphill site increases by more than 100%: the magnitude of the improved RE is comparable to those from the FVF and modified VGF methods and larger than that of the soil respiration independently measured by the chamber method (Lee et al., 2010; Chae, 2011; Lee, 2011). The F_{CO2_Obs} data between the times of $R_{sdn} > 0$ and the compensation point (i.e., when GPP = RE) are critical to estimating the LRC, especially its y-intercept (i.e., mean daytime RE). Such improvement shows that the site-specific filter works well in discarding the underestimated F_{CO2_Obs} around sunrise.

Table 1
Annually integrated ecosystem respiration (RE), gross primary production (GPP), and net ecosystem exchange (NEE) for the uphill (GDK) and downhill (GCK) sites in 2008, 2009, and 2010 without/with the site-specific DPN filter. The FVF, LRC, VGF, and AVG mean friction velocity filtering corrections, light response curve correction, modified van Gorsel correction methods, and their average value, respectively, are also listed. General theoretical filter means FVF, LRC, and VGF without the site-specific DPN filter (Units are g C m^{-2} per year).

		Uphill						Downhill					
		General theoretical filter			Site-specific DPN filter			General theoretical filter			Site-specific DPN filter		
		RE	GPP	NEE	RE	GPP	NEE	RE	GPP	NEE	RE	GPP	NEE
2008	FVF	1304	1393	−89	1472	1482	−9	1689	1845	−156	1867	1843	24
	LRC	460	943	−483	1004	1226	−222	1095	1532	−438	1439	1619	−179
	VGF	960	1221	−261	1468	1479	−11	1917	1983	−66	1541	1656	−115
	AVG	908 ± 424	1186 ± 227	−277 ± 198	1315 ± 269	1396 ± 147	−81 ± 122	1567 ± 425	1787 ± 231	−220 ± 194	1616 ± 224	1706 ± 120	−90 ± 104
2009	FVF	1323	1367	−44	1477	1434	43	1783	2062	−280	1789	1930	−141
	LRC	388	875	−487	918	1144	−226	1183	1757	−575	1802	1982	−180
	VGF	1078	1246	−168	1593	1500	93	2042	2253	−211	1902	1987	−85
	AVG	929 ± 485	1163 ± 256	−233 ± 229	1329 ± 361	1359 ± 189	−30 ± 172	1669 ± 441	2024 ± 250	−355 ± 193	1831 ± 62	1966 ± 32	−135 ± 48
2010	FVF	1416	1338	78	1439	1352	87	1787	2108	−321	2092	2148	−56
	LRC	405	813	−408	820	1041	−221	944	1645	−700	1527	1819	−292
	VGF	984	1129	−145	1333	1307	26	1953	2220	−267	1846	1977	−131
	AVG	935 ± 508	1093 ± 265	−158 ± 243	1197 ± 331	1233 ± 168	−36 ± 163	1561 ± 541	1991 ± 305	−430 ± 236	1822 ± 283	1981 ± 165	−160 ± 121

The underestimation (overestimation) of the modified VGF method for the uphill (downhill) site was also solved after application of the site-specific filter. In particular, the GPP at the downhill site in 2009 and 2010 decreased from $2237 \pm 23\,g\,C\,m^{-2}\,year^{-1}$ to $1982 \pm 7\,g\,C\,m^{-2}\,year^{-1}$, which is smaller than its upper limit ($\sim 2200\,g\,C\,m^{-2}\,year^{-1}$) from using the observed R_{sdn} ($GPP_{upper} = 0.47 R_{sdn} \cdot \eta_{photon} \cdot LUE \cdot fAPAR$, where 0.47 is the fraction of photosynthetically active radiation (PAR) to R_{sdn} (e.g., Britton and Dodd, 1976), η_{photon} is the conversion factor for energy-based PAR to photon-based PAR ($= 4.56\,\mu mol\,J^{-1}$; e.g., McCree, 1972), LUE is the light-use efficiency (approximated as 0.02 μmol C per μmol quanta; e.g., Lagergren et al., 2005), and fAPAR is the fraction of absorbed PAR (approximated as 0.9, which is the maximum in a vegetated area); the annual R_{sdn} values in both years are approximately $4800\,MJ\,m^{-2}\,year^{-1}$; Kang et al., 2014). The magnitude of GPP at the downhill site was still high, but acceptable considering that the downhill site is a densely planted coniferous forest with rapid growth (Kang, 2013).

The differences in the CO_2 budget between the nighttime correction methods for both sites decrease after the application of the site-specific filter: the decreasing percentage of the standard deviation among the annual sums of each component ranges from 25% to 38% for the uphill site and from 46% to 87% for the downhill site. However, the differences between the methods still remain even though the site-specific filter solves the discrepancy between the methods. In particular, there is a significant difference between the LRC method using daytime data to estimate the RE and the FVF method (and modified VGF) using nighttime data, suggesting that the difference in RE between daytime and nighttime at the same temperature is significant for both sites (e.g., Wohlfahrt et al., 2005; van Gorsel et al., 2009). The additional independent measurement of the CO_2 flux using a different method (e.g., chamber measurements) is not available, which could be used to judge the most appropriate method. Therefore, rather than preferentially trusting a result from a certain method, we propose to estimate the CO_2 budgets as the averages of the results from the three methods and use their standard deviation as the uncertainty of the nighttime correction for both sites.

It is a noteworthy validation that the uphill site is carbon neutral (or a weak carbon sink) after applying the site-specific DPN filter. This result is expected because the 500 year old uphill site has reached the climax forest stage of succession which is known as carbon neutral. In this forest we know there is an equilibrium between the amount of carbon released through decay of dead and diseased tree and the carbon absorbed (e.g., Kengen, 1997; Kang et al., 2014).

4. Summary and conclusions

This study provides a method for applying the information flow DPN approach to ascertain the advection of CO_2 via drainage flow at a hill slope tower site.

Vertical profile measurements of CO_2 concentrations at two tower sites demonstrated the following: (1) different patterns of CO_2 concentrations between the uphill and downhill site at night, (2) an underestimation (overestimation) of the NEE peaks around sunset for the uphill (downhill) site, and (3) asymmetric magnitudes of F_{CO2_Obs} around sunset and sunrise. Based on these results, we identified that (1) the drained CO_2 from the uphill site banks up to the downhill site and (2) the CO_2 drainage continues until early morning, when the valley wind blows.

Using the information flow DPN, we have delineated the characteristics of CO_2 drainage such as timing, temporal scale, direction, and structure. The key findings include the following: (1) the drained CO_2 strongly accumulates from 17:00 to 21:00 regardless of season; (2) the primary timescale of that drainage process is one half hour; (3) the accumulated CO_2 does not dissipate uphill; (4) the more the canopy develops, the more clearly the CO_2 flows are divided into two parts, i.e., above and below the canopy; and (5) the traditional u^* threshold can successfully filter out the drainage-affected data from 17:00 to 21:00.

Based on the above findings, we developed a site-specific quality control filter that eliminates the F_{CO2_Obs} significantly affected by the drainage of CO_2. The filter discards the data (1) when the CO_2 drainage is fully generated as the mountain wind prevails (i.e., 21:00 to 9:00, 8:00, and 7:30 for the dormant, transition, and growing seasons, respectively), (2) when u^* is lower than the threshold ($0.3\,m\,s^{-1}$) while the drainage flow is under strong development (from 17:00 to 21:00), and (3) until the accumulated CO_2 completely dissipates for the downhill site (i.e., before noon).

The site-specific filter improves the discrepancy between the three nighttime correction methods (i.e., FVF, LRC, and the modified VGF) and the inconsistency between the EC measurement and the other measurement/estimation (e.g., soil respiration measured by the chamber method, upper gross primary production limited by radiation). This site-specific filter has an equivalent effect of the application of the two (or three) nighttime correction methods in a hybrid way. However, our method has some weaknesses: (1) CO_2 measurements are needed at two or more sites along the drainage, (2) a long-term dataset is necessary to produce a reliable results, and (3) the time resolution of the result is not fine. Some of these weakness can be resolved if a shorter averaging time (e.g., 5 or 10 min) of the CO_2 concentration profile measurements is used, resulting in larger sample sizes and a finer timescale. This will allow us to resolve differences in advection due to rapidly varying forcing meteorology in more temporal detail (Barr and Orgill, 1989; Gudiksen et al., 1992).

This method can be applied using sub-canopy measurements of CO_2 concentration if there are at least two concentration measurements- one uphill and one downhill at an appropriate distance. A pair of concentration measurements near ground level is much easier to collect than above-canopy measurements and profiles, or multi-site EC data, but is nevertheless effective because as we have shown the peaks of net transfer entropy between the sites occur near the soil surface in the lower layers (Fig. 8). Roughly two to four meters, or about 10% of the canopy's height, is an appropriate height above the soil surface for the concentration measurements in this forest.

The 'Moving Point Test' (MPT, Gu et al., 2005), an automated statistical method based on an iterative approach using a moving window for u^*, is widely used to determine the u^* threshold. In a future study, we hope to develop a modified MPT method using moving windows for 'time' as well as u^*, which can determine the 'timing when CO_2 drainage is generated' as well as the u^* threshold for application to single-flux tower measurements.

In addition, we expect that this method can be applied to ascertain not only the advection of CO_2 but also that of latent/sensible heat and other properties affected by advection. The annual surface energy balance ratio ($EBR = \Sigma(LE + H) / \Sigma R_{net}$) assumes that annual ground heat flux and storage flux are negligible, where LE is the latent heat flux, H is the sensible heat flux (H), and R_{net} is the net radiation. 1 of EBR means that surface energy budget is closed. The EBR terms (Wilson et al., 2002) are 0.66–0.67 and for the uphill site and 1.05–1.12 for the downhill site (Kang, 2013). It suggests that there might be the advected latent/sensible heat from the uphill to the downhill in similar fashion to the CO_2 advection- and if so, this method could be used to filter those processes as well.

It is the authors' hope that this paper's methods will find broad applications to the identification of advection using read-

ily available concentration and state observations in a wide range of applications.

Acknowledgments

This work was supported by the Korea Meteorological Administration Research and Development Program under Grant KMIPA 2015-2023, and Weather Information Service Engine (WISE) project, KMA-2012-0001-A. Dr. Benjamin L. Ruddell's contribution to this research was supported by the National Science Foundation under Grant No. EF-1241960. We thank Hyojung Kwon, Jinkyu Hong, Jaeill Yoo, Bindu Malla Thakuri, Juyeol Yun, Boeun Choi, and Je-woo Hong for their helpful support of the data collection and other logistics. The findings are those of the authors, and not necessarily the funding agencies or broader team members.

Appendix A. Test of the methodology

To test whether our methodology works properly, we apply the method to a test case as follows.

$$X_1 = A_1(\sin(t+9)/24 \cdot 2\pi) + \varepsilon_1)$$

$$X_2 = A_2(\sin(t+9)/24 \cdot 2\pi) + \varepsilon_2)$$

$$Y_1 = A_1(\sin(t+9)/24 \cdot 2\pi) + \varepsilon_3)$$

$$Y_2 = A_2(\sin(t+9)/24 \cdot 2\pi) + \varepsilon_4)$$

$$X'_{1,t} = \frac{\partial X_{1,t}}{\partial t} \approx \frac{\Delta X_{1,t}}{\Delta t} = \frac{X_{1,t} - X_{1,t-1}}{\Delta t}$$

$$X'_{2,t} = \frac{\partial X_{2,t}}{\partial t} - \alpha_t \approx \frac{\Delta X_{2,t}}{\Delta t} - \alpha_t = \frac{X_{2,t} - X_{2,t-1}}{\Delta t} - \alpha_t$$

$$Y'_{1,t} = \frac{\partial Y_{1,t}}{\partial t} + \alpha_{1,t-1} \approx \frac{\Delta Y_{1,t}}{\Delta t} + \alpha_{1,t-1} = \frac{Y_{1,t} - Y_{1,t-1}}{\Delta t} + \alpha_{1,t-1}$$

$$Y'_{2,t} = \frac{\partial Y_{2,t}}{\partial t} + \alpha_{2,t-1} \approx \frac{\Delta Y_{2,t}}{\Delta t} + \alpha_{2,t-1} = \frac{Y_{2,t} - Y_{2,t-1}}{\Delta t} + \alpha_{2,t-1} \quad \text{(A1)}$$

where A_1 and A_2 are 0.85 and 1, respectively; subscripts 1 and 2 indicate the different layers; t is the time (hour, time step is one half hour); $\varepsilon_{(1,2,3,4)}$ is a random number between −0.5 and 0.5 with uniform distribution; and α_t is the sum of $\alpha_{1,t}$ and $\alpha_{2,t}$. $\alpha_{1,t}$ and $\alpha_{2,t}$ are

$$\alpha_{1,t} = \begin{cases} \dfrac{C_1 \Delta X_{2,t}}{\Delta t}, \text{ when } 17:00 \le t < 21:00 \\ 0, \text{ when } t < 17:00 \text{ or } t \ge 21:00 \end{cases}$$

$$\alpha_{2,t} = \begin{cases} \dfrac{C_2 \Delta X_{2,t}}{\Delta t}, \text{ when } 17:00 \le t < 21:00 \\ 0, \text{ when } t < 17:00 \text{ or } t \ge 21:00 \end{cases} \quad \text{(A2)}$$

where A_1 and A_2 are 0.2 and 0.3, respectively. We generate the synthetic time series of X_1', X_2', Y_1', and Y_2' and calculate T' the same as for the case of this study. According to Eqs. (A1) and (A2), we expected a high $T'(X_2' \to Y_1', 30\,\text{min})$ and $T'(X_2' \to Y_2', 30\,\text{min})$ from approximately 17:00 to 21:00 (the time is the middle of the time window for calculating T'). As expected, we could identify the peaks of $T'(X_2' \to Y_1', 30\,\text{min})$ and $T'(X_2' \to Y_2', 30\,\text{min})$ from approximately 17:00 to 21:00, which could not be identified in other pairs, time lags, or timings (Fig. A1a and b). The magnitudes of the T' peaks correspond to the magnitudes of the coefficients, C_1 and C_2. The T's other than the T' peaks are non-zero, and their magnitude depends on the magnitude of the variability for each pair. Therefore, if we use a net T', we can more clearly distinguish the information flow generated by advection. We also confirmed that $\Sigma\Delta$ is useful in detecting the timing of CO_2 advection from uphill to downhill (Fig. A1c and d). However, the $\Sigma T'$ ($X' \to Y'$) at 22:00 is higher than its $\Sigma\Delta$, despite

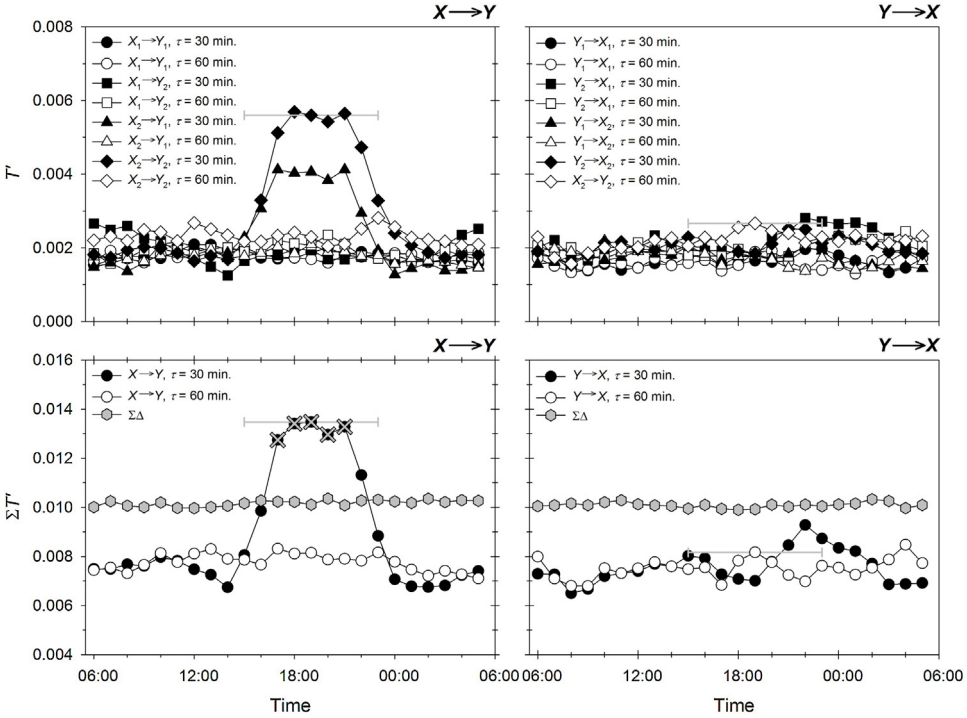

Fig. A1. Synthetic example: diurnal variation of the transfer entropy (T') from X to Y ($X \to Y$; a) with time lags and vice versa ($Y \to X$; b); the integrated T' ($\Sigma T'$) and its statistical significance ($\Sigma\Delta$) (c and d). Horizontal bars indicate the time window size for quantifying T' (8 h). X marks indicate the integrated T' larger than the empirical criterion (C_E).

the lack of physical flow at that time due to the eight-hour time window at 22:00 still including the signal from 18:00 to 21:00.

To overcome this shortcoming, we additionally apply the empirical criterion (C_E) for detecting the time of advection:

$$C_E = \Sigma T'_{\max} - \Delta\Sigma T'$$
$$\Delta\Sigma T' = \alpha(\Sigma T'_{\max} - \Sigma T'_{\text{base}}) \quad \text{(A3)}$$

where $\Sigma T'_{\max}$ is the maximum $\Sigma T'$ when the magnitude of CO_2 advection is maximum, $\Sigma T'_{\text{base}}$ is the base $\Sigma T'$ when the CO_2 advection is negligible ($\Sigma T'$ at approximately noon, $\Sigma T'$ at 12:00 in this study), and α is the empirical coefficient. Considering the window size (8 h) and the duration of CO_2 advection in the study sites (4–5 h, see Sections 3.1 and 3.2), the α value of 0.25 is a good parameter for distinguishing the timing of advection. Actually, the C_E in this test case can successfully identify the duration of the process (Fig. A1c and d). Overall, we conclude that this method is appropriate for characterizing the timing, direction, relative strength, temporal scale, and structure of CO_2 advection.

References

Aubinet, M., Chermanne, B., Vandenhaute, M., Longdoz, B., Yernaux, M., Laitat, E., 2001. Long term carbon dioxide exchange above a mixed forest in the Belgian Ardennes. Agric. For. Meteorol. 108, 293–315.

Aubinet, M., Feigenwinter, C., Heinesch, B., Bernhofer, C., Canepa, E., Lindroth, A., Montagnani, L., Rebmann, C., Sedlak, P., Van Gorsel, E., 2010. Direct advection measurements do not help to solve the night-time CO_2 closure problem: evidence from three different forests. Agric. For. Meteorol. 150, 655–664.

Aubinet, M., 2008. Eddy covariance CO_2 flux measurements in nocturnal conditions: an analysis of the problem. Ecol. Appl. 18, 1368–1378.

Baldocchi, D., Hicks, B.B., Meyers, T.P., 1988. Measuring biosphere-atmosphere exchanges of biologically related gases with micrometeorological methods. Ecology 69, 1331–1340.

Baldocchi, D., Falge, E., Wilson, K., 2001. A spectral analysis of biosphere–atmosphere trace gas flux densities and meteorological variables across hour to multi-year time scales. Agric. For. Meteorol. 107, 1–27.

Barr, S., Orgill, M.M., 1989. Influence of external meteorology on nocturnal valley drainage winds. J. Appl. Meteorol. 28, 497–517.

Britton, C., Dodd, J., 1976. Relationships of photosynthetically active radiation and shortwave irradiance. Agric. Meteorol. 17, 1–7.

Brooks, A., Farquhar, G.D., 1985. Effects of temperature on the CO_2/O_2 specificity of ribulose-1,5-bisphosphate carboxylase/oxygenase and the rate of respiration in the light. Planta 165, 397–406.

Campbell Scientific Inc, 2003. 8 Level CO_2 and H_2O Profile System Operation Manual. Campbell Scientific Inc.

Campbell, G., Norman, J.M., 1998. An Introduction to Environmental Biophysics. Springer, New York, pp. 66–74.

Chae, N., 2011. Annual variation of soil respiration and precipitation in a temperate forest (*Quercus serrata* and *Carpinus laxiflora*) under east asian monsoon climate. J. Plant Biol. 54, 101–111.

Falge, E., Baldocchi, D., Olson, R., Anthoni, P., Aubinet, M., Bernhofer, C., Burba, G., Ceulemans, R., Clement, R., Dolman, H., 2001. Gap filling strategies for defensible annual sums of net ecosystem exchange. Agric. For. Meteorol. 107, 43–69.

Feigenwinter, C., Bernhofer, C., Vogt, R., 2004. The influence of advection on the short term CO_2 budget in and above a forest canopy. Boundary-Layer Meteorol. 113, 201–224.

Finnigan, J., 2004. A re-evaluation of long-term flux measurement techniques part II: coordinate systems. Boundary-Layer Meteorol. 113, 1–41.

Gu, L., Falge, E.M., Boden, T., Baldocchi, D.D., Black, T., Saleska, S.R., Suni, T., Verma, S.B., Vesala, T., Wofsy, S.C., 2005. Objective threshold determination for nighttime eddy flux filtering. Agric. For. Meteorol. 128, 179–197.

Gudiksen, P.H., Leone, J.M., King, C.W., Ruffieux, D., Neff, W.D., 1992. Measurements and modeling of the effects of ambient meteorology on nocturnal drainage flows. J. Appl. Meteorol. 31, 1023–1032.

Hong, J., Lee, D., Kim, J., 2005. Lessons from FIFE (First ISLSCP Field Experiment) in scaling issues of surface fluxes at Gwangneung supersite. Korean J. Agric. For. Meteorol. 7, 4–14 (in Korean with English abstract).

Hong, J., Kim, J., Lee, D., Lim, J.-H., 2008. Estimation of the storage and advection effects on H_2O and CO_2 exchanges in a hliily KoFlux forest catchment. Water Resour. Res. 44, W01426.

Hong, J., Kwon, H.-J., Lim, J.-H., Byun, Y.-H., Lee, J.-H., Kim, J., 2009. Standardization of KoFlux eddy-covariance data processing. Korean J. Agric. For. Meteorol. 11, 19–26 (in Korean with English abstract).

Kang, M., Park, S., Kwon, H., Choi, H.T., Choi, Y.-J., Kim, J., 2009. Evapotranspiration from a deciduous forest in a complex terrain and a heterogeneous farmland under monsoon climate. Asia-Pac. J. Atmos. Sci. 45, 175–191.

Kang, M., Kwon, H., Cheon, J.H., Kim, J., 2012. On estimating wet canopy evaporation from deciduous and coniferous forests in the asian monsoon climate. J. Hydrometeorol. 13, 950–965.

Kang, M., Kim, J., Kim, H.-S., Thakuri, B.M., Chun, J.-H., 2014. On the nighttime correction of CO_2 flux measured by eddy covariance over temperate forests in complex terrain. Korean J. Agric. For. Meteorol. 16, 233–245 (in Korean with English abstract).

Kang, M., Kim, J., Chun, J.-H., Boo, K.-O, Cho, C.H., 2016. Improvement and expansion of standardized KoFlux eddy covariance data processing protocol (in preparation).

Kang, M., 2013. Understanding the Evapotranspiration Dynamics in East Asian Forest Ecosystems for Resilient Water Management. PhD Dissertation. Yonsei University.

Kengen, S., 1997. Forest Valuation for Decision-making: Lessons of Experience and Proposals for Improvement. FAO.

Kim, J., Lee, D., Hong, J., Kang, S., Kim, S.-J., Moon, S.-K., Lim, J.-H., Son, Y., Lee, J., Kim, S., Woo, N., Kim, K., Lee, B., Lee, B.-L., Kim, S., 2006. HydroKorea and CarboKorea: cross-scale studies of ecohydrology and biogeochemistry in a heterogeneous and complex forest catchment of Korea. Ecol. Res. 21, 881–889.

Kumar, P., Ruddell, B.L., 2010. Information driven ecohydrologic self-organization. Entropy 12, 2085–2096.

Kwon, H., Park, T.-Y., Hong, J., Lim, J.-H., Kim, J., 2009. Seasonality of net ecosystem carbon exchang in two major plant functional types in Korea. Asia-Pac. J. Atmos. Sci. 45, 149–163.

Lagergren, F., Eklundh, L., Grelle, A., Lundblad, M., Mölder, M., Lankreijer, H., Lindroth, A., 2005. Net primary production and light use efficiency in a mixed coniferous forest in Sweden. Plant Cell Environ. 28, 412–423.

Lee, J.S., 2011. Monitoring soil respiration using an automatic operating chamber in a Gwangneung temperate deciduous forest. J. Ecol. Environ. 34, 411–422.

Lee, X., Fuentes, J.D., Staebler, R.M., Neumann, H.H., 1999. Long-term observation of the atmospheric exchange of CO_2 with a temperate deciduous forest in southern Ontario, Canada. J. Geophys. Res. Atmos. 104, 15975–15984.

Lee, N.-y., Koo, J.-W., Noh, N.J., Kim, J., Son, Y., 2010. Autotrophic and heterotrophic respiration in needle fir and *Quercus*-dominated stands in a cool-temperate forest, central Korea. J. Plant Res. 123, 485–495.

Leuning, R., Zegelin, S.J., Jones, K., Keith, H., Hughes, D., 2008. Measurement of horizontal and vertical advection of CO_2 within a forest canopy. Agric. For. Meteorol. 148, 1777–1797.

Lloyd, J., Taylor, J., 1994. On the temperature dependence of soil respiration. Funct. Ecol. 8, 315–323.

Malla Thakuri, B., Kang, M., Chun, J.-H., Kim, J., 2016. Vertical profiles of CO_2 concentrations and storage in temperate forests in Korea (in preparation).

Marcolla, B., Cescatti, A., Montagnani, L., Manca, G., Kerschbaumer, G., Minerbi, S., 2005. Role of advective fluxes in the carbon balance of an alpine coniferous forest. Agric. For. Meteorol. 130, 193–206.

McCree, K.J., 1972. Test of current definitions of photosynthetically active radiation against leaf photosynthesis data. Agric. Meteorol. 10, 443–453.

McMillen, R.T., 1988. An eddy correlation technique with extended applicability to non-simple terrain. Boundary-Layer Meteorol. 43 (3), 231–245.

Novick, K., Brantley, S., Miniat, C.F., Walker, J., Vose, J.M., 2014. Inferring the contribution of advection to total ecosystem scalar fluxes over a tall forest in complex terrain. Agric. For. Meteorol. 185, 1–13.

Papale, D., Reichstein, M., Aubinet, M., Canfora, E., Bernhofer, C., Kutsch, W., Longdoz, B., Rambal, S., Valentini, R., Vesala, T., Yakir, D., 2006. Towards a standardized processing of net ecosystem exchange measured with eddy covariance technique: algorithms and uncertainty estimation. Biogeosciences 3 (4), 571–583.

Reichstein, M., Falge, E., Baldocchi, D., Papale, D., Aubinet, M., Berbigier, P., Bernhofer, C., Buchmann, N., Gilmanov, T., Granier, A., Grunwald, T., Havrankova, K., Ilvesniemi, H., Janous, D., Knohl, A., Laurila, T., Lohila, A., Loustau, D., Matteucci, G., Meyers, T., Miglietta, F., Ourcival, J.-M., Pumpanen, J., Rambal, S., Rotenberg, E., Sanz, M., Tenhunen, J., Seufert, G., Vaccari, F., Vesala, T., Yakir, D., Valentini, R., 2005. On the separation of net ecosystem exchange into assimilation and ecosystem respiration: review and improved algorithm. Global Change Biol. 11, 1424–1439.

Ruddell, B.L., Kumar, P., 2009a. Ecohydrologic process networks: 1. Identification. Water Resour. Res. 45, W03419.

Ruddell, B.L., Kumar, P., 2009b. Ecohydrologic process networks: 2. Analysis and characterization. Water Resour. Res. 45, W03420.

Schreiber, T., 2000. Measuring information transfer. Phys. Rev. Lett. 85, 461–464.

Shannon, C.E., 1948. A mathematical theory of communication. Bell Syst. Tech. J. 27, 379–423.

van Gorsel, E., Leuning, R., Cleugh, H.A., Keith, H., Suni, T., 2007. Nocturnal carbon efflux: reconciliation of eddy covariance and chamber measurements using an alternative to the u*-threshold filtering technique. Tellus Ser. B-Chem. Phys. Meteorol. 59, 397–403.

van Gorsel, E., Leuning, R., Cleugh, H.A., Keith, H., Kirschbaum, M.U., Suni, T., 2008. Application of an alternative method to derive reliable estimates of nighttime respiration from eddy covariance measurements in moderately complex topography. Agric. For. Meteorol. 148, 1174–1180.

van Gorsel, E., Delpierre, N., Leuning, R., Black, A., Munger, J.W., Wofsy, S., Aubinet, M., Feigenwinter, C., Beringer, J., Bonal, D., 2009. Estimating nocturnal ecosystem respiration from the vertical turbulent flux and change in storage of CO_2. Agric. For. Meteorol. 149, 1919–1930.

Webb, E.K., Pearman, G.I., Leuning, R., 1980. Correction of flux measurements for density effects due to heat and water vapour transfer. Q. J. R. Meteorol. Soc. 106 (447), 85–100.
Wilczak, J., Oncley, S., Stage, S., 2001. Sonic anemometer tilt correction algorithms. Boundary-Layer Meteorol. 99, 127–150.
Wilson, K., Goldstein, A., Falge, E., Aubinet, M., Baldocchi, D., Berbigier, P., Bernhofer, C., Ceulemans, R., Dolman, H., Field, C., Grelle, A., Ibrom, A., Law, B.E., Kowalski, A., Meyers, T., Moncrieff, J., Monson, R., Oechel, W., Tenhunen, J., Valentini, R., Verma, S., 2002. Energy balance closure at FLUXNET sites. Agric. For. Meteorol. 113, 223–243.
Wohlfahrt, G., Bahn, M., Haslwanter, A., Newesely, C., Cernusca, A., 2005. Estimation of daytime ecosystem respiration to determine gross primary production of a mountain meadow. Agric. For. Meteorol. 130, 13–25.
Yi, C., Anderson, D.E., Turnipseed, A.A., Burns, S.P., Sparks, J.P., Stannard, D.I., Monson, R.K., 2008. The contribution of advective fluxes to net ecosystem exchange in a high-elevation, subalpine forest. Ecol. Appl. 18, 1379–1390.
Yoo, J.-I., Lee, D.-H., Hong, J.-K., Kim, J., 2009. Principles and applications of multi-level H_2O/CO_2 profile measurement system. Korean J. Agric. For. Meteorol. 11, 27–38 (in Korean with English abstract).
Yuan, R., Kang, M.-S., Park, S.-B., Hong, J.-K., Lee, D.-H., Kim, J., 2007. The effect of coordinate rotation on the eddy covariance flux estimation in a hilly KoFlux forest catchment. Korean J. Agric. For. Meteorol. 9, 100–108.
Yuan, R., Kang, M., Park, S.-B., Hong, J., Lee, D., Kim, J., 2011. Expansion of the planar-fit method to estimate flux over complex terrain. Meteorol. Atmos. Phys. 110, 123–133.